Science Advances

AAAS

advances.sciencemag.org/cgi/content/full/2/4/e1501290/DC1

Supplementary Materials for

TIE2-mediated tyrosine phosphorylation of H4 regulates DNA damage response by recruiting ABL1

Mohammad B. Hossain, Rehnuma Shifat, David G. Johnson, Mark T. Bedford, Konrad R. Gabrusiewicz, Nahir Cortes-Santiago, Xuemei Luo, Zhimin Lu, Ravesanker Ezhilarasan, Erik P. Sulman, Hong Jiang, Shawn S. C. Li, Frederick F. Lang, Jessica Tyler, Mien-Chie Hung, Juan Fueyo, Candelaria Gomez-Manzano

Published 1 April 2016, *Sci. Adv.* **2**, e1501290 (2016)
DOI: 10.1126/sciadv.1501290

The PDF file includes:

- Table S3. List of antibodies used for this study.

SUPLEMENTARY FIGURES

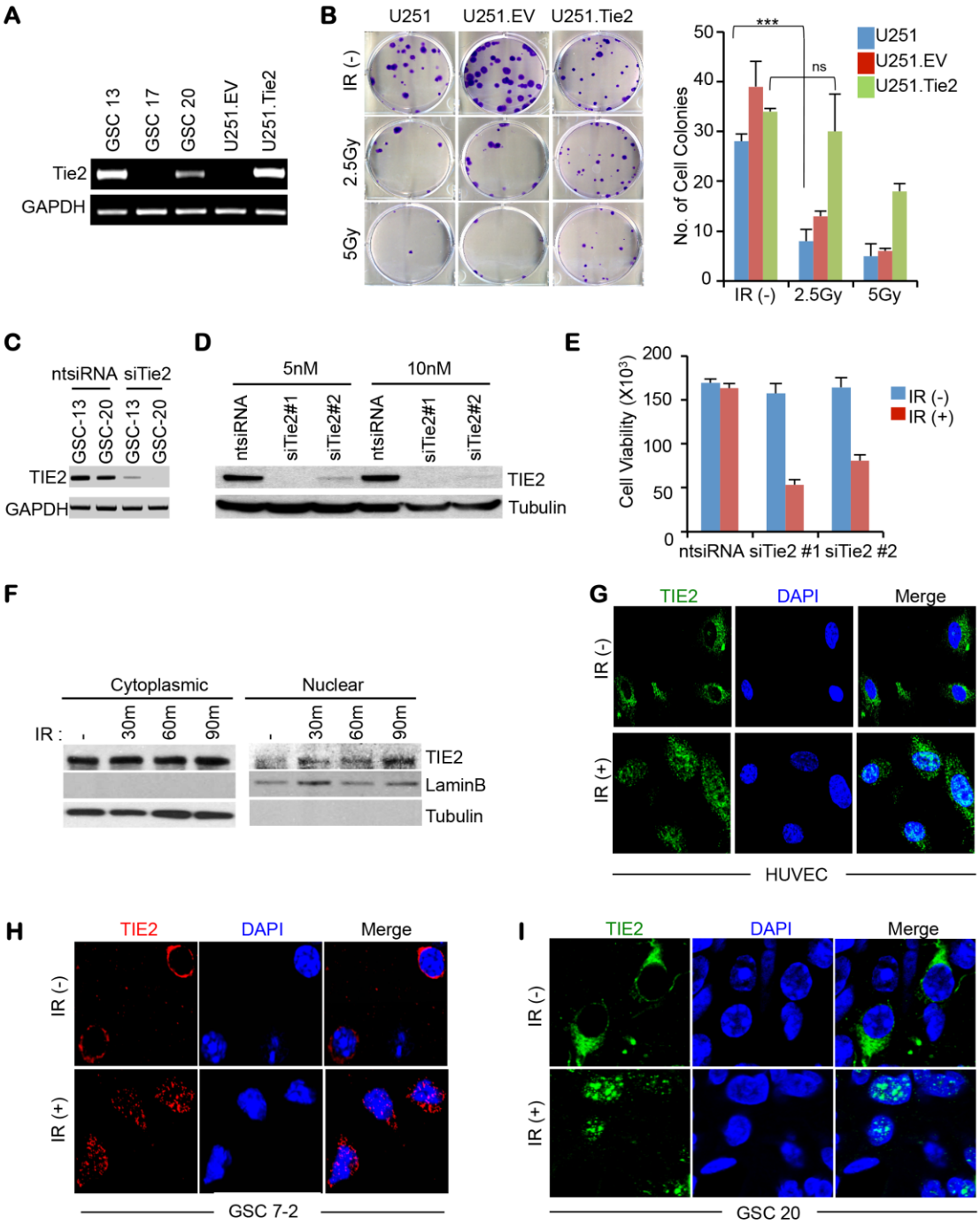

Figure S1. Additional analyses on TIE2 nuclear expression and glioma radioresistance

fig. S1. Additional analyses on TIE2 nuclear expression and glioma radioresistance. (**A**) TIE2 expression in glioma stem cell (GSC) lines was analyzed by semi-quantitative RT-PCR. U251.EV and U251.Tie2 glioma cell lines were used as the negative and positive controls for TIE2 expression, respectively. GAPDH expression levels were used as loading control. (**B**) Clonogenic assay in U251.P, U251.EV and U251.Tie2 cells after ionizing radiation (IR: 2.5Gy and 5.0Gy). Data represent mean ± s.d.; ns, $P > 0.05$, ***$P \leq 0.001$. (**C,D**) siRNA against TIE2 effectively decreases TIE2 expression levels in (**C**) GSCs and (**D**) U251.Tie2 cells. (**E**) TIE2 silencing results in the radiosensitization of U251.Tie2 cultures. (**F**) TIE2 subcellular localization after IR treatment of HUVECs, in a time point experiment. LaminB and Tubulin were used as nuclear and cytoplasmic protein loading controls, respectively. (**G**) Confocal analysis of HUVECs with and without IR demonstrating TIE2 translocation to nucleus. (**H,I**) Confocal microscopy images showing TIE2 nuclear localization in immunofluorescence-stained sections of brains of irradiated mice bearing intracranial (**H**) GSC 7-2 and (**I**) GSC 20 xenografts.

A

[1]MDSLASLVLCGVSLLLSGTVEGAMDLILINSLPLVSDAETSLTCIASGWRPHEPITIGRDFEAL
MNQHQDPLEVTQDVTREWAKKVVWKREKASKINGAYFCEGRVRGEAIRIRTMKMRQQASFLPAT
LTMTVDKGDNVNISFKKVLIKEEDAVIYKNGSFIHSVPRHEVPDILEVHLPHAQPQDAGVYSAR
YIGGNLFTSAFTRLIVRRCEAQKWGPECNHLCTACMNNGVCHEDTGECICPPGFMGRTCEKACE
LHTFGRTCKERCSGQEGCKSYVFCLPDPYGCSCATGWKGLQCNEACHPGFYGPDCKLRCSCNNG
EMCDRFQGCLCSPGWQGLQCEREGIPRMTPKIVDLPDHIEVNSGKFNPICKASGWPLPTNEEMT
LVKPDGTVLHPKDFNHTDHFSVAIFTIHRILPPDSGVWVCSVNTVAGMVEKPFNISVKVLPKPL
NAPNVIDTGHNFAVINISSEPYFGDGPIKSKKLLYKPVNHYEAWQHIQVTNEIVTLNYLEPRTE
YELCVQLVRRGEGGEGHPGPVRRFTTASIGLPPPRGLNLLPKSQTTLNLTWQPIFPSSEDDFYV
EVERRSVQKSDQQNIKVPGNLTSVLLNNLHPREQYVVRARVNTKAQGEWSEDLTAWTLSDILPP
QPENIKISNITHSSAVISWTILDGYSISSITIRYKVQGKNEDQHVDVKIKNATIIQYQLKGLEP
ETAYQVDIFAENNIGSSNPAFSHELVTLPESQAPADLGGGKMLLIAILGSAGMTCLTVLLAFLI
ILQLKRANVQRRMAQAFQNVREEPAVQFNSGTLALNRKVKNNPDPTIYPVLDWNDIKFQDVIGE
GNFGQVLKARIKKDGLRMDAAIKRMKEYASKDDHRDFAGELEVLCKLGHHPNIINLLGACEHRG
YLYLAIEYAPHGNLLDFLRKSRVLETDPAFAIANSTASTLSSQQLLHFAADVARGMDYLSQKQF
IHRDLAARNILVGENYVAKIADFGLSRGQEVYVKKTMGRLPVRWMAIESLNYSVYTTNSDVWSY
GVLLWEIVSLGGTPYCGMTCAELYEKLPQGYRLEKPLNCDDEVYDLMRQCWREKPYERPSFAQI
LVSLNRMLEERKTYVNTTLYEKFTYAGIDCSAEEAA[1124]

NLS Motif : [580]*RRSVQKS*[586]

B

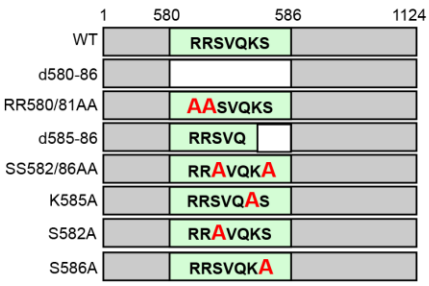

C

Color key for alignment scores between *Tie1* and *Tie2*

D

TIE1 ***508*** RLWDGARGQERRENVSSPQARTA-LLAGLTPGTHYQLDVRLYHCTLLGPASPPARVLLPP ***566***
TIE2 ***577*** EVERRSVQKSDQQNIKVPGNLTSVLLNNLHPREQYVVRARVNTKAQGEWSEDLTAWTLSD ***636***

Figure S2. TIE2 nuclear translocation signal

fig. S2. TIE2 nuclear translocation signal. (**A**) Predicted NLS motif in *Tie2*, ^{580}*RRSVQKS*^{586}, is highlighted in red. (**B**) Schematic diagram of mutant constructs spanning the predicted *Tie2* NLS (^{580}RRSVQKS^{586}). (**C**) DNA nucleotide sequence alignment of *Tie1* and *Tie2* showing the percentage of homology between the two TIE receptors. (**D**) DNA nucleotide sequence alignment of the *Tie2* NLS sequence (red box) with Tie1.

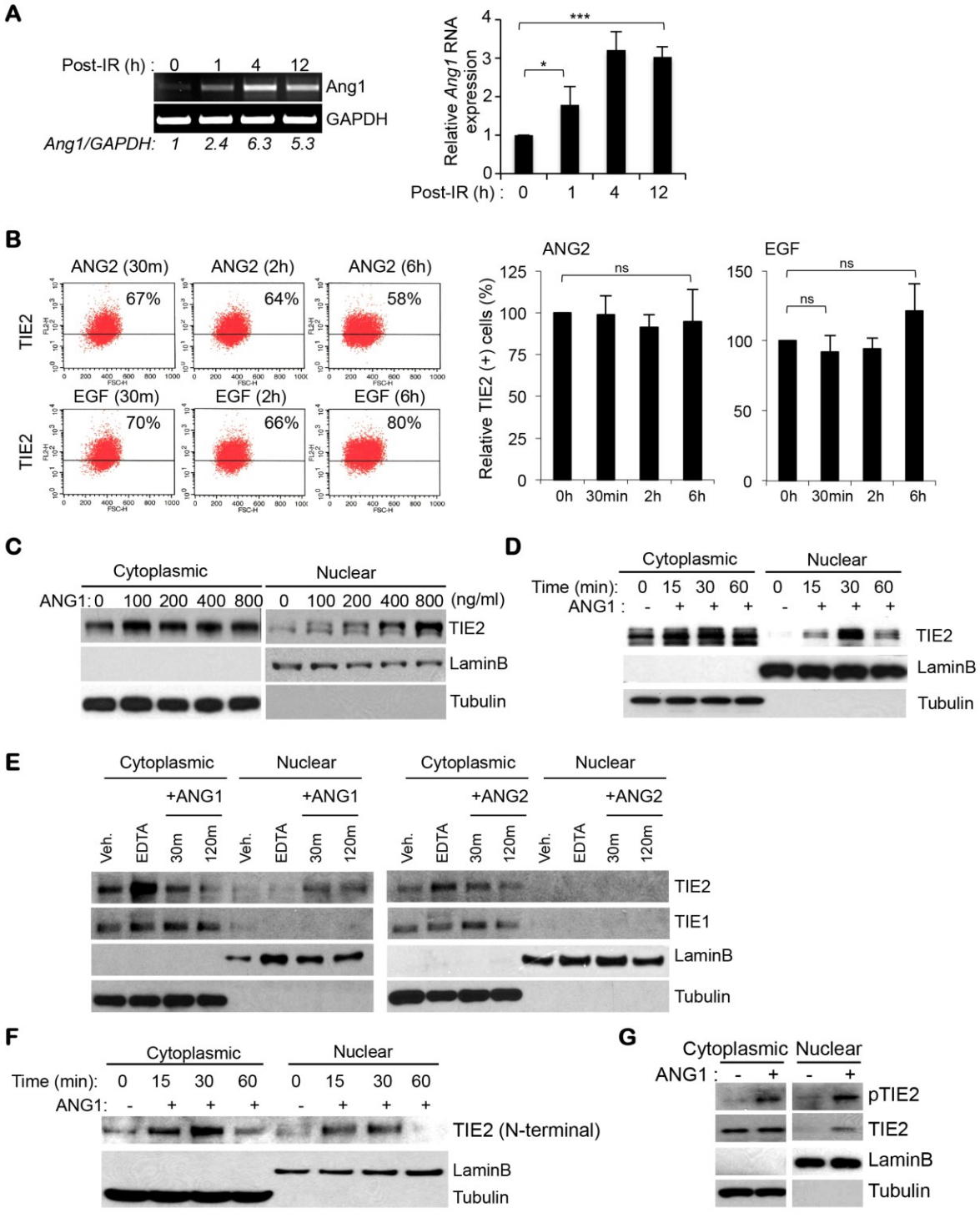

Figure S3. ANG1 regulates TIE2 nuclear translocation

fig. S3. **ANG1 regulates TIE2 nuclear translocation**. (**A**) IR (10Gy) modifies *Ang1* mRNA levels as assessed by RT-PCR (left) and qRT-PCR (right). Data are presented as fold increase of the relative ratio Ang1/GAPDH (RT-PCR) and Ang1/Actin (qRT-PCR). Densitometry was performed using the NIH public available ImageJ software. **P* < 0.05, ***P* <0.001. (**B**) Exposure to ANG2 (400 ng/ml) or EGF (20 ng/ml) did not modify the cellular membrane TIE2 expression levels in U251.Tie2 glioma cells. The percentage of TIE2-positive cells was quantified using FACS analysis. Data represent mean ± s.d.; ns, *P* > 0.05. (**C**) ANG1 exposure of U251.Tie2 cultures resulted in TIE2 nuclear translocation in a dose-dependent experiment, as assessed by subcellular fractionation and Western blotting. LaminB and Tubulin were used as nuclear and cytoplasmic protein loading controls, respectively. (**D**) Endogenous TIE2-expressing HUVECs were similarly analyzed for TIE2 translocation upon ANG1 in a time-dependent experiment. LaminB and Tubulin were used as nuclear and cytoplasmic protein loading controls, respectively. (**E**) ANG1 exposure of HUVECs did not result in Tie1 nuclear translocation, as assessed by subcellular fractionation and Western blot analysis. EDTA (0.1 M) was used as a negative stimulator for the movement of TIE2 to the nucleus. (**F**) ANG1-induced nuclear TIE2 subcellular localization in U251.Tie2 cells was also observed using an antibody targeted to the N-terminal region of the protein. (**G**) Nuclear TIE2 was phosphorylated (Y992) upon ANG1 treatment of U251.Tie2 cells, as assessed by subcellular fractionation and Western blotting. LaminB and Tubulin were used as nuclear and cytoplasmic protein loading controls, respectively.

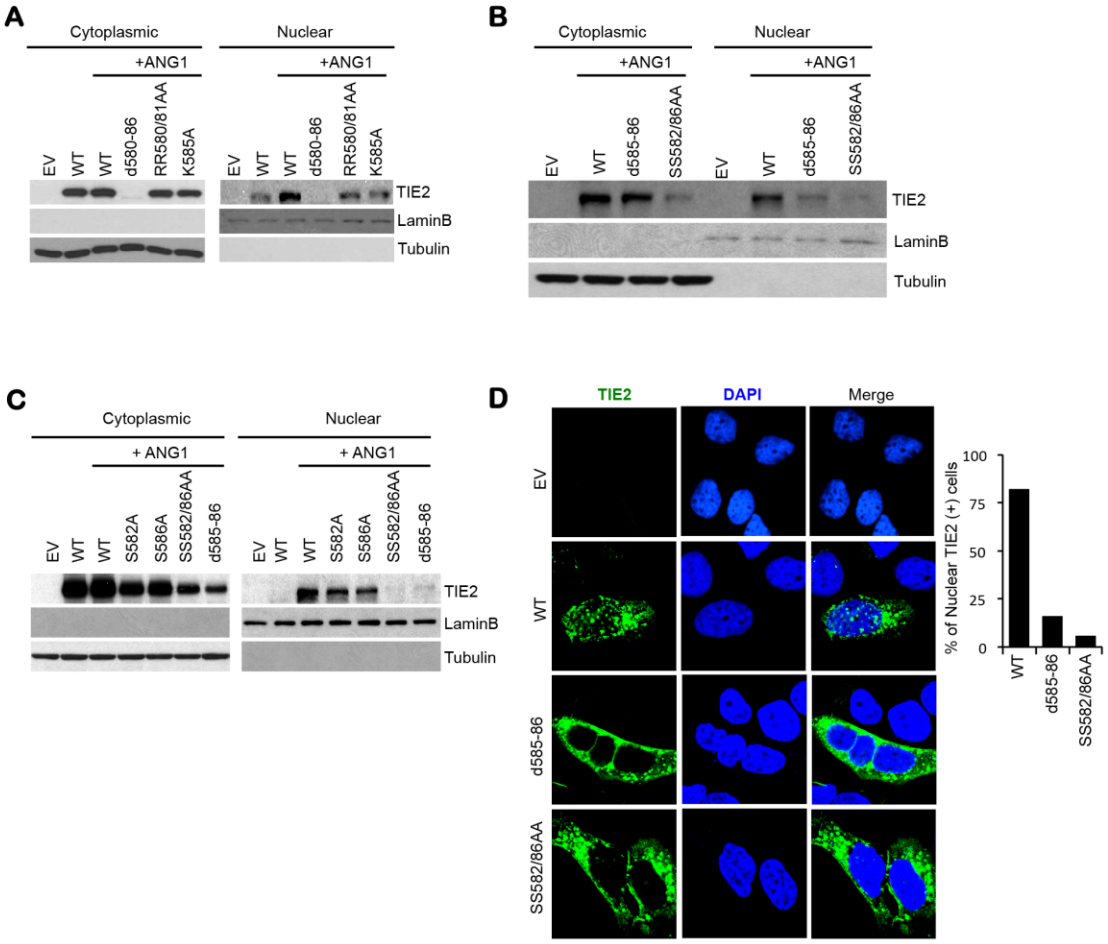

Figure S4. S582 and S586 may modulate TIE2 nuclear translocation

fig. S4. S582 and S586 may modulate TIE2 nuclear translocation. (**A to C**) TIE2 subcellular localization after ANG1 exposure of (**A**) HeLa cells, (**B**) HEK293 cells, and (**C**) U251 cells after 48 h of transfection with the indicated mutant *Tie2* expression constructs, as assessed by Western blotting. LaminB and Tubulin were used as nuclear and cytoplasmic protein loading controls, respectively. (**D**) HEK293 cells were plated at low confluency in chamber slides and transfected with d585-86 or SS582/86AA mutant *Tie2*. 48 h later, the cultures were exposed to ANG1. Shown here are the representative confocal images of the immunofluorescence analysis and the quantification of the percentage of cells expressing nuclear TIE2.

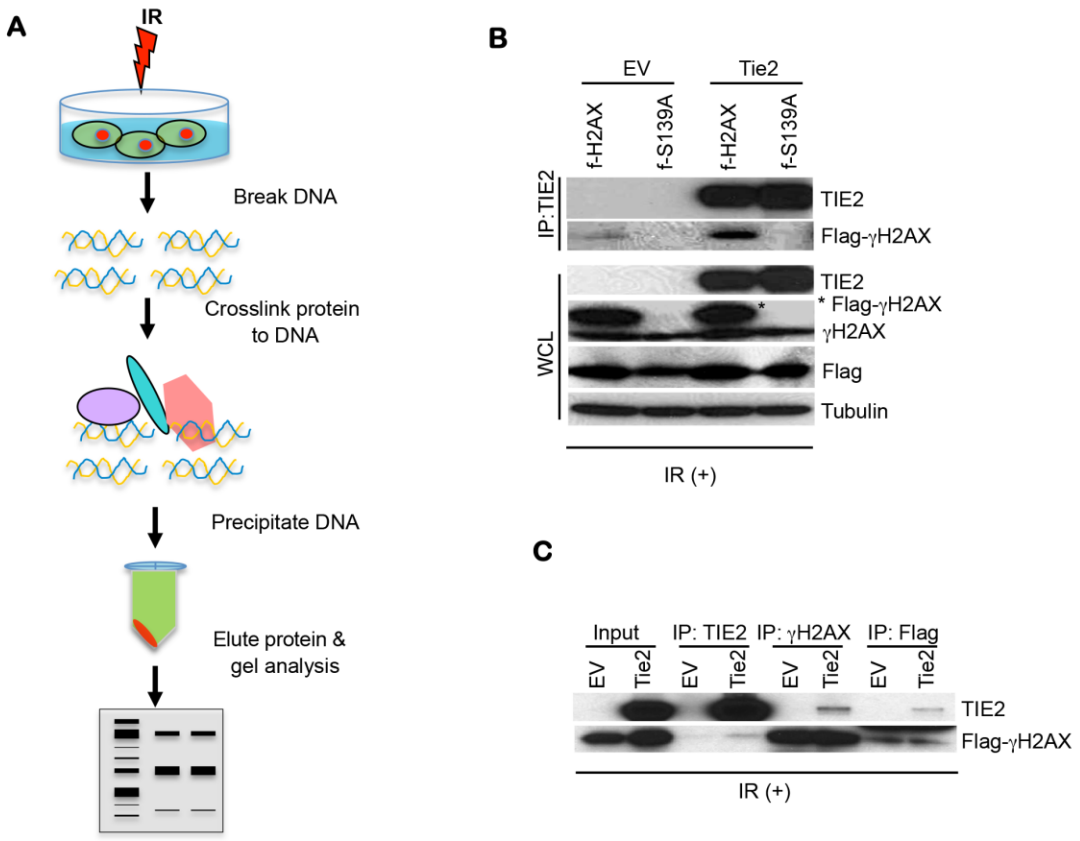

Figure S5. Additional analyses on nuclear TIE2 binding γH2AX complexes

fig. S5. **Additional analysis on nuclear TIE2 binding γH2AX complexes.** (**A**) Schematic diagram of DNA-bound protein isolation methodology. Cells were irradiated and cross-linked, and DNA was precipitated. DNA-bound proteins were isolated and identified using Western blot analysis. (**B**) Flag-tagged, H2AX-overexpressing HEK293 cell lines [f-H2AX (WT) and f-S139A H2AX (mutant)] were transfected with *pCDNA.EV* or *pCDNA.Tie2* vectors. 48 h later, cells were treated with IR (10Gy) and incubated for 1 h. Cell extracts were immunoprecipitated with anti-TIE2 antibody and immunoblotted as indicated. (**C**) Flag-tagged H2AX-overexpressing HEK293 cell lines [f-H2AX (WT)] were transfected with *pCDNA.EV* and *pCDNA.Tie2* vectors. 48 h later, cells were treated with IR and incubated for 1 h. Cell extracts were immunoprecipitated with anti-TIE2, anti-γH2AX, or anti-Flag antibodies and immunoblotted as indicated.

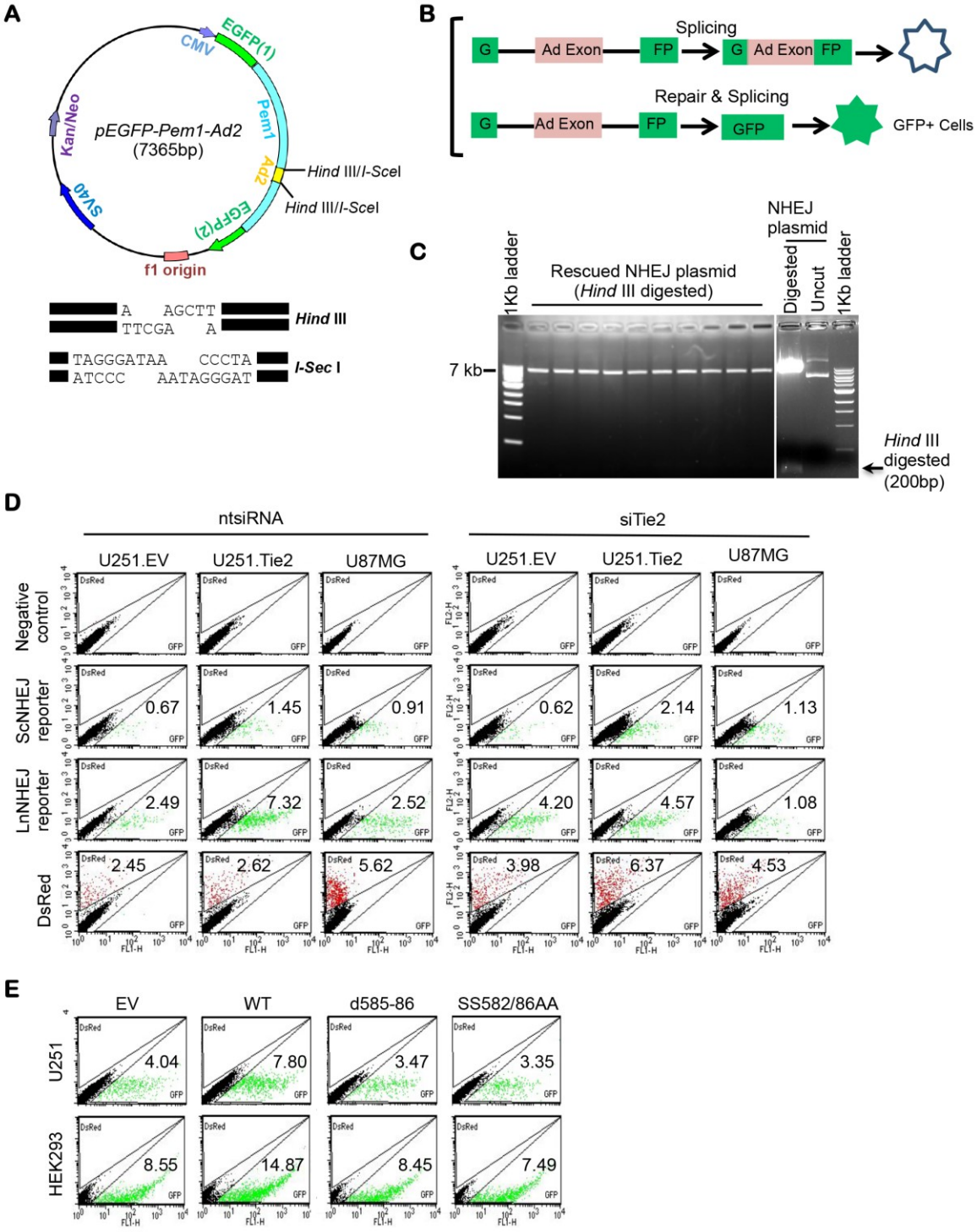

Figure S6. Additional analysis on the role of nuclear TIE2 in the regulation of DNA repair via NHEJ (*Hind* III)

fig. S6. **Additional analysis of the role of nuclear TIE2 in the regulation of DNA repair via NHEJ (Hind III).** (**A**) Shown here is the circular map of reporter plasmid *pEGFP-Pem1-Ad2* diagram. The EGFP gene is interrupted by a stuffer sequence containing an Ad2 exon. Endonuclease sites are marked. As depicted, digestion with *I-Sce*I or *Hind*III generates noncompatible or cohesive NHEJ substrates, respectively. (**B**) Schematic representation of the restoration of EGFP expression after successful intracellular plasmid circularization. The presence of the Ad-exon in the middle of the Pem1 intron inactivates EGFP activity and creates the starting EGFP-negative substrate. After removing the Ad exon intracellular plasmid circularization, EGFP expression is restored and can be quantitated by flow cytometry analysis. (**C**) Rescued circular plasmids from U251.Tie2 cells previously transfected with *Hind*III-linearized pEGFP-Pem1-Ad2 were analyzed by agarose gel electrophoresis, after restriction digestion with *Hind*III. Uncut and *Hind*III-digested pEGFP-Pem1-Ad2 plasmids were loaded as controls. (**D**) The efficiency of NHEJ in irradiated U251.Tie2 and U87MG cells was analyzed by FACS-guided quantification of EGFP-positive cells normalized to Ds-Red-positive cells. The role of TIE2 in NHEJ repair was analyzed using siRNA against TIE2 (5nM). (**E**) The role of nuclear TIE2 in NHEJ repair was analyzed by quantifying EGFP-positive cells, via FACS, in irradiated U251 and HEK293 cell lines previously transfected with mutant *Tie2* constructs (d585-86 and SS582/86AA).

A

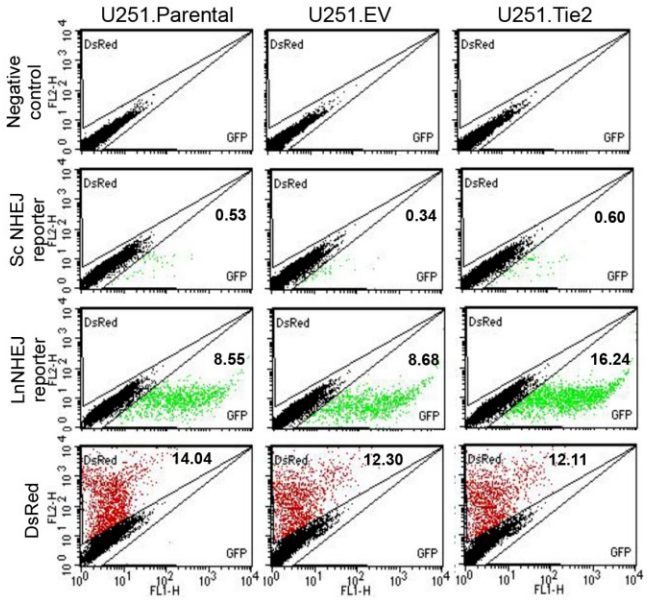

B

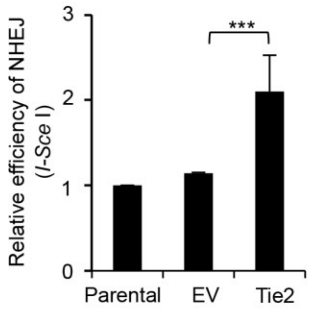

Figure S7. Additional analysis on the role of nuclear TIE2 in the regulation of DNA repair via NHEJ (*I-Sce* I)

fig. S7. Additional analysis of the role of nuclear TIE2 in the regulation of DNA repair via NHEJ (I-Sce I). (**A**) The efficiency of NHEJ in irradiated U251.P, U251.EV, and U251.Tie2 cells transfected *I-Sce*I-linearized *pEGFP-Pem1-Ad2* was analyzed by FACS-guided quantification. Shown is a representative experiment. (**B**) Quantification of EGFP-positive cells normalized to Ds-Red-positive cells. Data represent mean ± s.d. ***P<0.001.

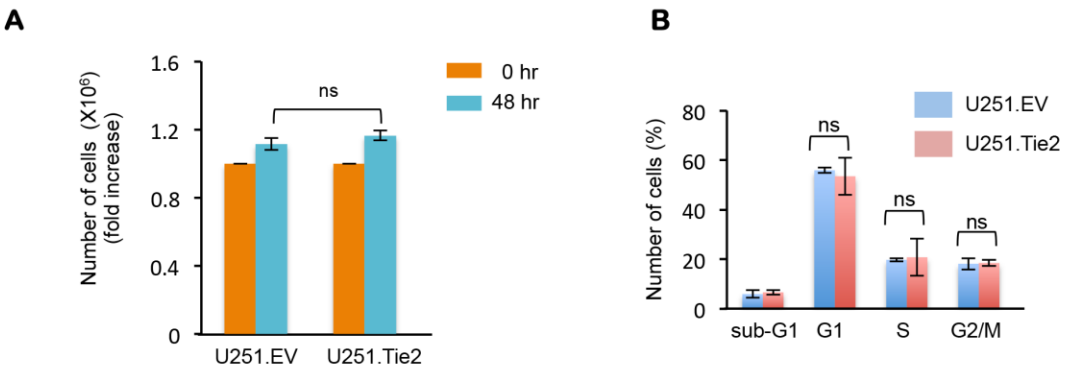

Figure S8. Analysis of Tie2 expression and cell cycle

fig. S8. Analysis of the relation of Tie2 expression and cell cycle. (**A** and **B**) U251.EV and U251.Tie2 cell number (A) and cell cycle distribution (B) were analyzed after 48 hr of plating cells in subconfluent conditions. Data represent mean ± s.d. ns, $P > 0.05$.

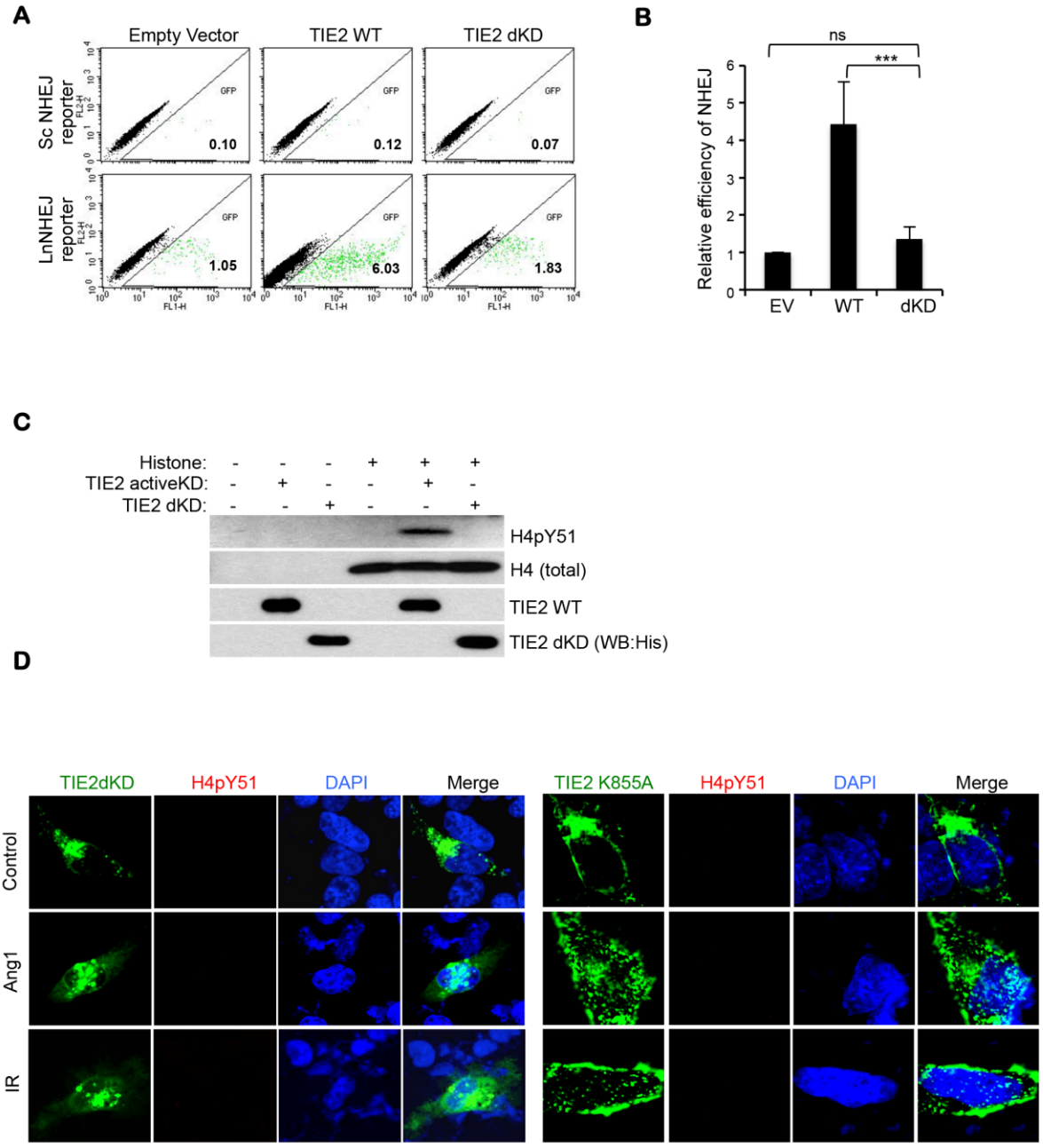

Figure S9. Tie2 kinase domain is essential for Tie2-mediated H4Y51 and NHEJ repair

fig. S9. Kinase activity of TIE2 is required for TIE2-mediated NHEJ repair. (**A** and **B**) The role of TIE2 in NHEJ repair in irradiated U251 cells previously transfected with wild-type *Tie2* (Tie2 WT) or *Tie2* with deleted kinase domain (Tie2 dKD) was analyzed by FACS-guided quantification of EGFP-positive cells normalized to Ds-Red-positive cells. (A) Shown is a representative experiment. (B) Data represent mean ± s.d. of triplicate experiments. ***P < 0.001, ns, P > 0.05. (**C** and **D**) TIE2 catalytic function is essential for H4Y51 phosphorylation, as shown by performing kinase assay followed by western blot analysis (**C**) and by immunofluorescence (**D**). Confocal analysis was performed to analyze the phosphorylation of H4Y51 in U251 cells transfected with the deleted kinase domain (TIE2dKD) or point mutation that results in death kinase function (TIE2K855A). U251 cells were plated subconfluent in a chamber slide and starved for 4 h. Cells were stained with TIE2 (green) and H4pY51 (red) after treatment with ANG1 and IR stimuli and assessed by confocal microscopy.

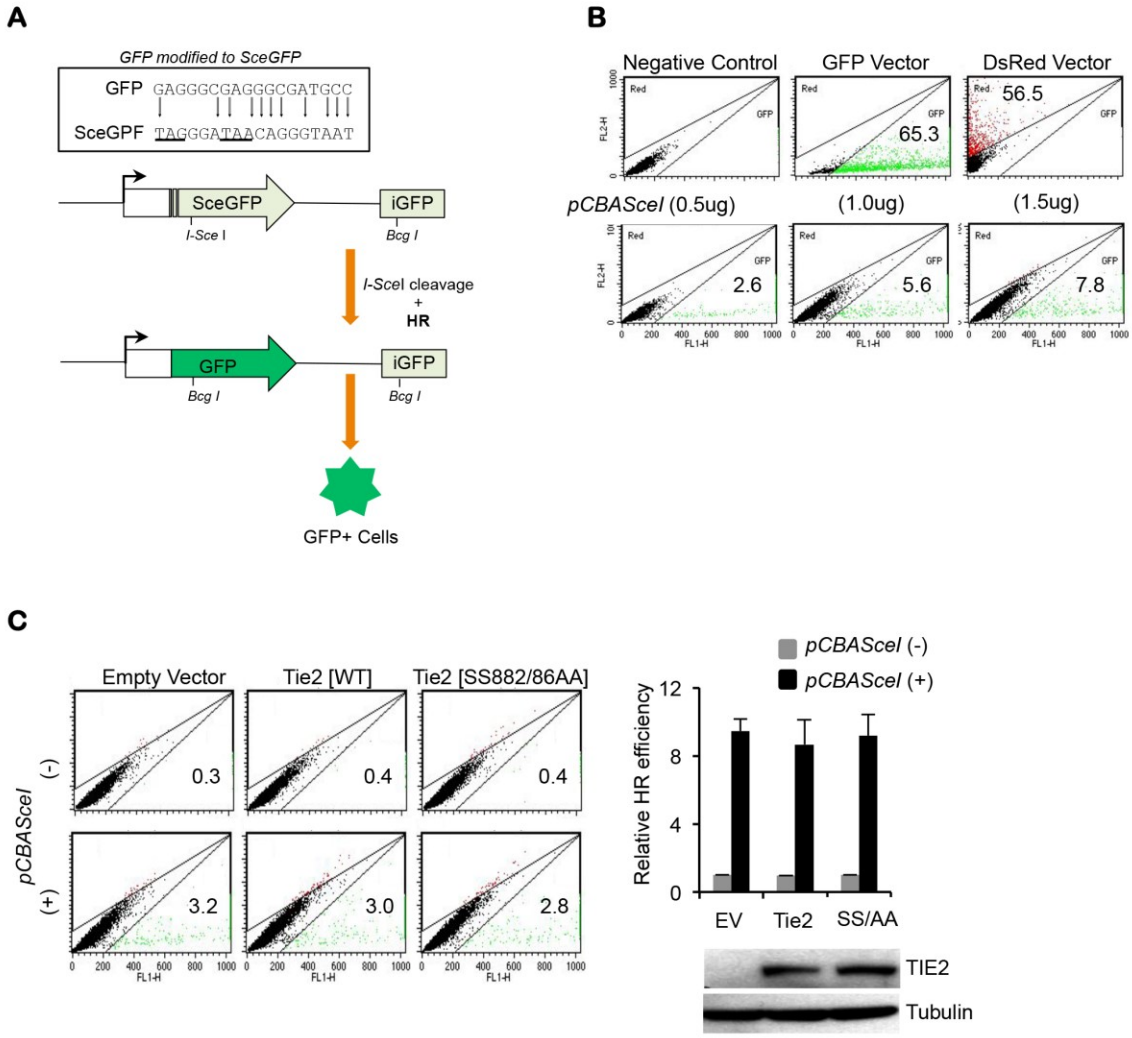

Figure S10. Nuclear TIE2 is not involved in DNA repair via HR

fig. S10. Nuclear TIE2 is not involved in DNA repair via HR. (**A**) Schematic diagram of the DR-GFP reporter system to measure DSB-induced HR. The cellular expression of *I-Sce*I leads to a DSB that can be repaired by HR using the wild-type GFP sequence as a template, resulting in GFP+ cells. (**B**) Titration of the *pCBASceI* plasmid in U2OS.DR-GFP cells for HR efficiency after IR. *pEGFP* and *pDsRed2-C1* plasmids were used for transfection efficiency. (**C**) HR efficiency in irradiated U2OS.DR-GFP cells was analyzed after transfection with wild-type and mutant *Tie2* expression vector constructs. Quantification of GFP-positive cells was normalized to Ds-Red-positive cells. U251.EV cells were used as a negative control for TIE2 expression. Data represent mean ± s.d.

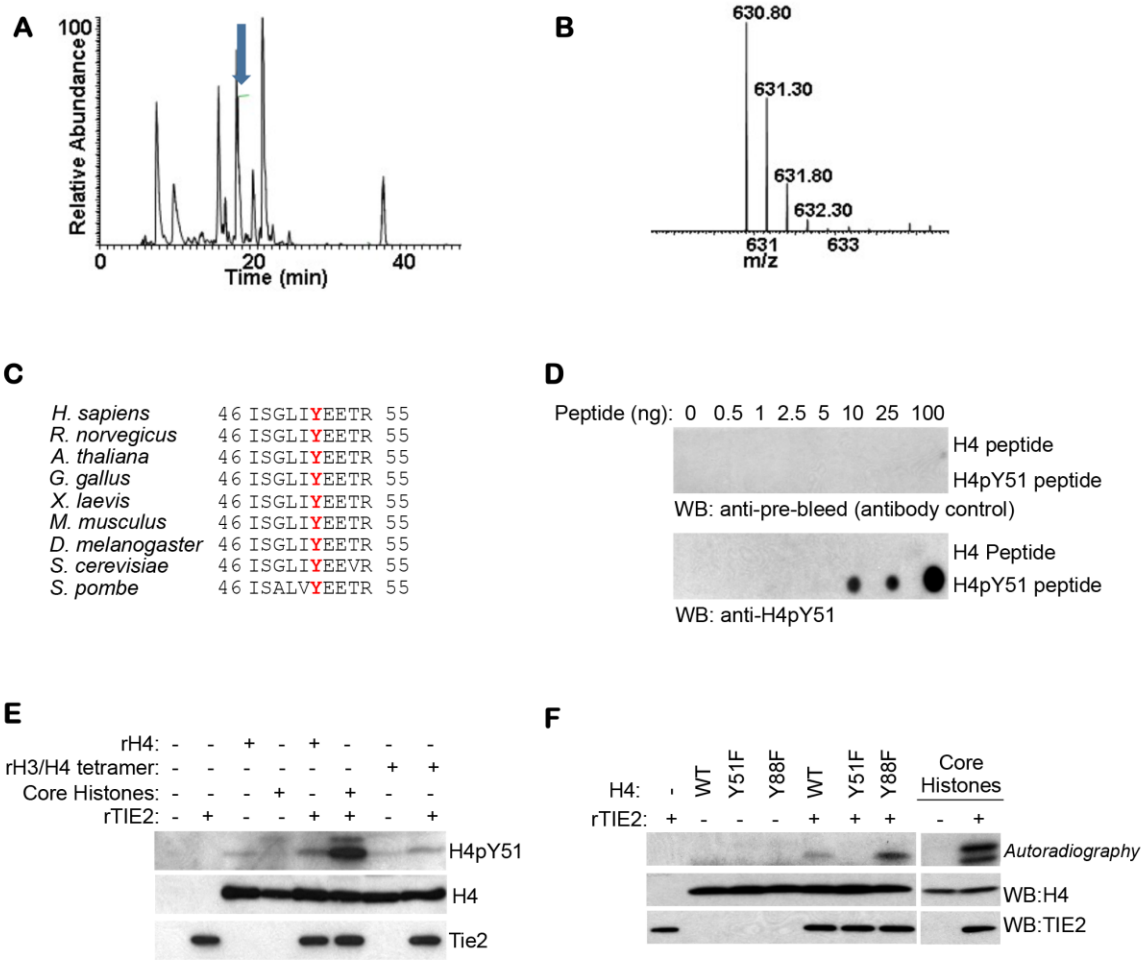

Figure S11. Additional analyses on the TIE2-mediated phosphorylation of the conserved Tyr51 residue in H4

fig. S11. Additional analyses on the TIE2-mediated phosphorylation of the conserved Tyr51 residue in H4. (**A**) Nano HPLC chromatograph of the histone H4 protein tryptic peptide mixture; the target ion was eluted as indicated (arrow). (**B**) A zoom scan of the target ion at 630.80Da shows that it is doubly charged. (**C**) H4Y51 (noted in red) is highly conserved among different species. (**D**) The histone H4 (H4Y51: GLIYEETRGVL) and phospho H4 (H4pY51: GLIpYEETRGVL) peptides were dotted at different concentrations onto nitrocellulose membranes and immunoblotted using pre-bleed serum (antibody control; top panel) or H4pY51 antibody (bottom panel). (**E**) TIE2-mediated H4 phosphorylation was analyzed after *in vitro* kinase assays involving rH4, rH3/H4 tetramers or core histones. Immunoblotting for levels of H4pY51 is shown. (**F**) Specificity of Tyr51 phosphorylation in H4 by TIE2 was analyzed using an in vitro kinase assay with purified wild-type and mutant H4 proteins. Immunoblotting for the presence of total H4 and TIE2 levels is shown.

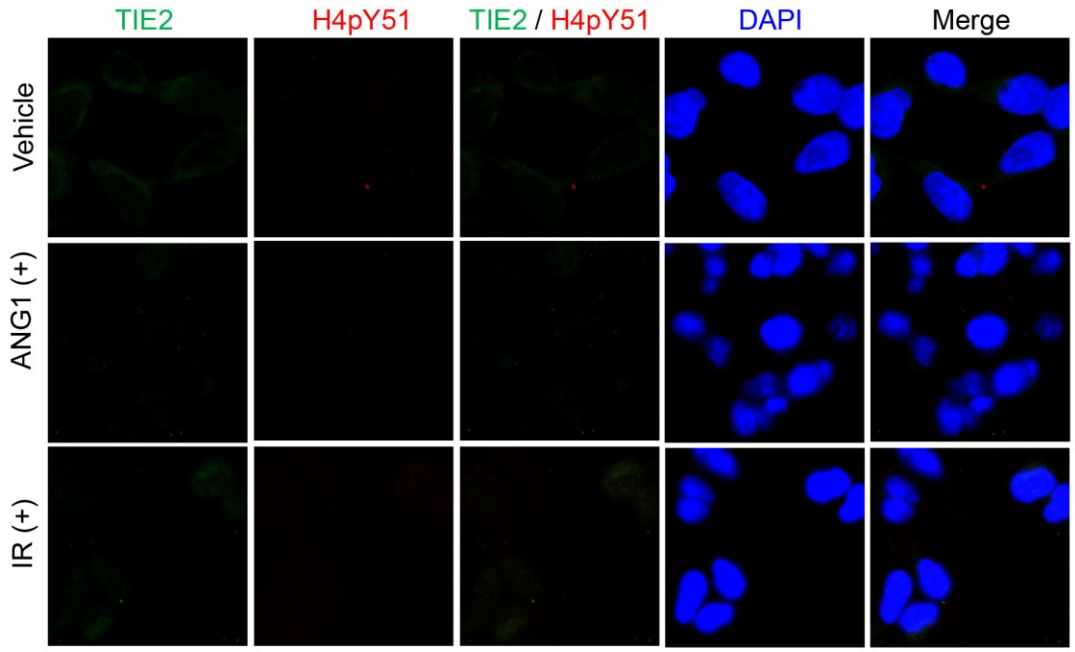

Figure S12. Additional analysis on TIE2/H4Y51 complexes in TIE2-negative cells

fig. S12. Additional analysis on TIE2/H4pY51 complexes in TIE2-negative cells. TIE2 is a specific kinase for H4Y51 phosphorylation. Confocal analysis was performed to analyze the phosphorylation of H4Y51 in non-TIE2-expressing cells. HEK293.EV cells were plated in a chamber slide with low confluency and starved for 4 h. Cells were stained with TIE2 (green) and H4pY51 (red) after treatment with ANG1 and IR stimuli and assessed by confocal microscopy.

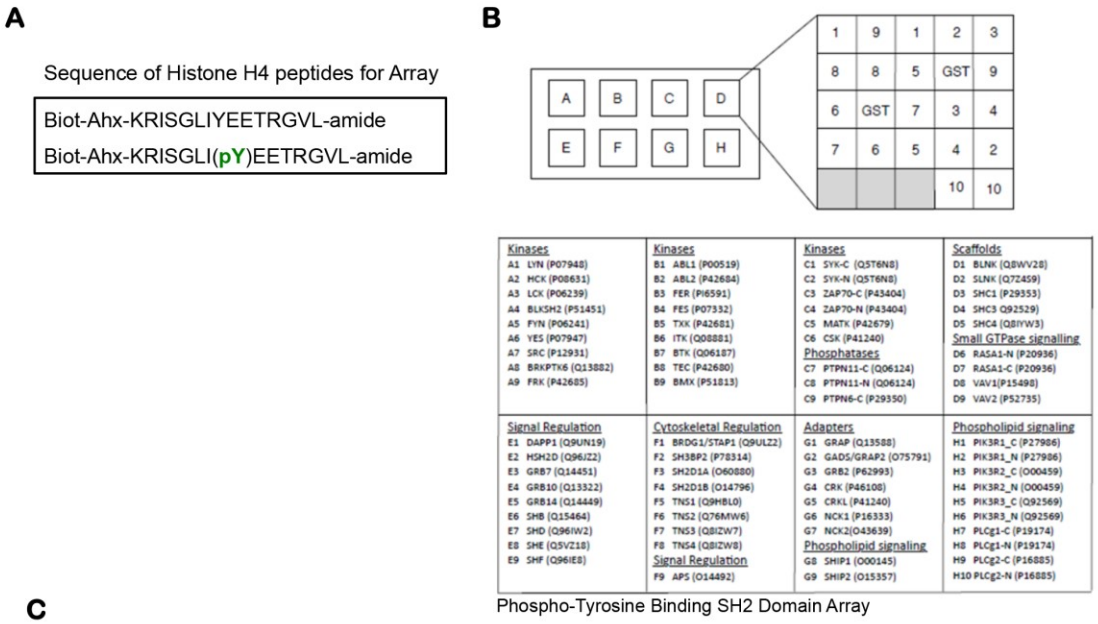

Figure S13. Additional analysis on H4Y51 reader

fig. S13. Additional analysis on H4Y51 reader. (**A**) Sequence of histone H4 peptides used for the SH2 domain binding array. (**B**) List of the specific SH2 domains present in the phospho-tyrosine binding array. (**C**) GST-tagged recombinant SH2 domains were arrayed onto nitrocellulose-coated glass slides and probed with the non-phospho H4 peptide (top) and phospho H4 peptide (bottom) described in (**A**). A fluorescent signal indicates binding of the phospho H4 peptide to the SH2 domains of ABL1, ABL2, VAV2, PIK3R1_N, PIK3R2_N, and PIK3R3_N (red highlighted).

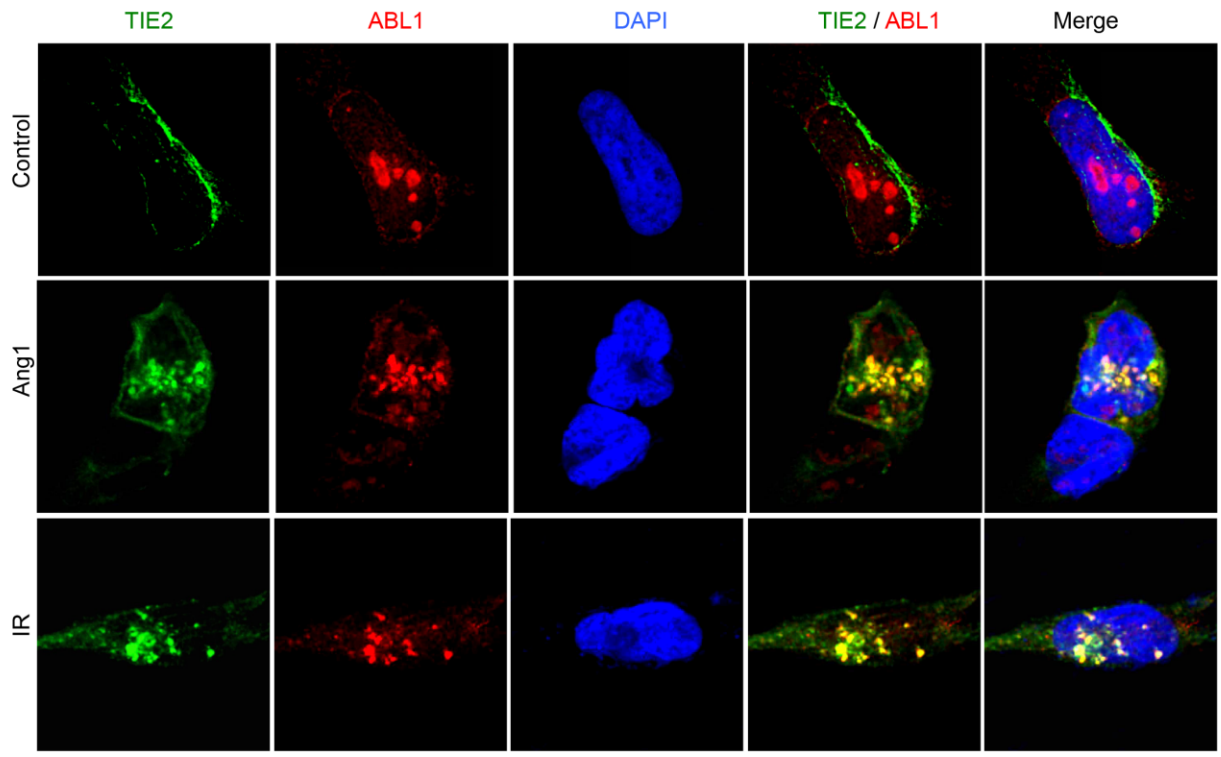

Figure S14. Additional analysis on Tie2/ABL1 complexes upon Ang1 or IR

fig. S14. Additional analysis on TIE2/ABL1 complexes upon ANG1 or IR. Confocal analysis was performed to analyze the formation of TIE2/ABL1 complexes in cells after IR or ANG1 stimulus. HEK293.Tie2.myc cells were plated in a chamber slide with low confluency and starved for 4 h. Cells were stained with TIE2 (green) and ABL1 (red) after treatment with ANG1 and IR stimuli and assessed by confocal microscopy.

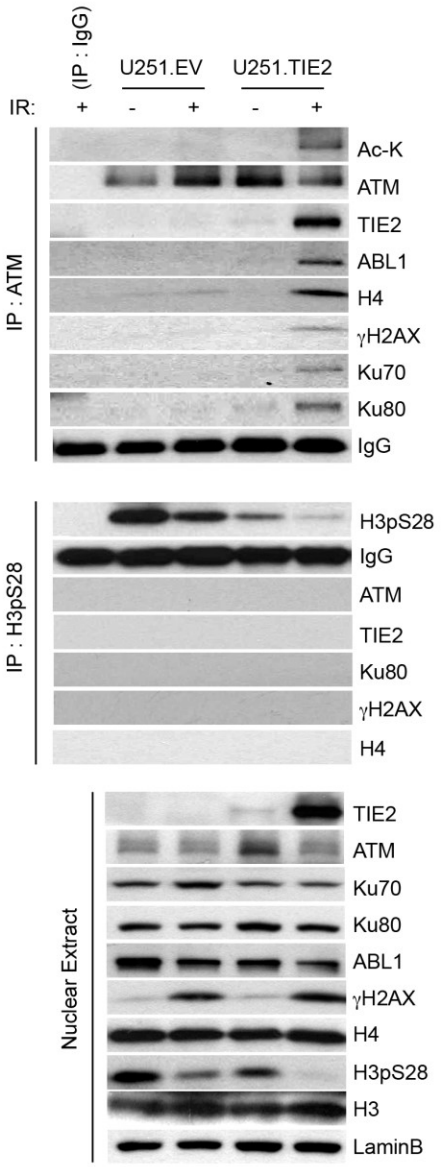

Figure S15. Additional analyses on nuclear TIE2/DNA Repair complexes

fig. S15. Additional analyses on nuclear TIE2/DNA repair complexes. ATM complexes with TIE2 and a panel of DNA repair proteins, including ABL1, in U251.EV and U251.Tie2-myc cells after IR exposure. Negative results after H3pS28 immunoprecipitation in those cells are also presented as specificity of the TIE2/H4Y51 complexes (Fig. 4K).

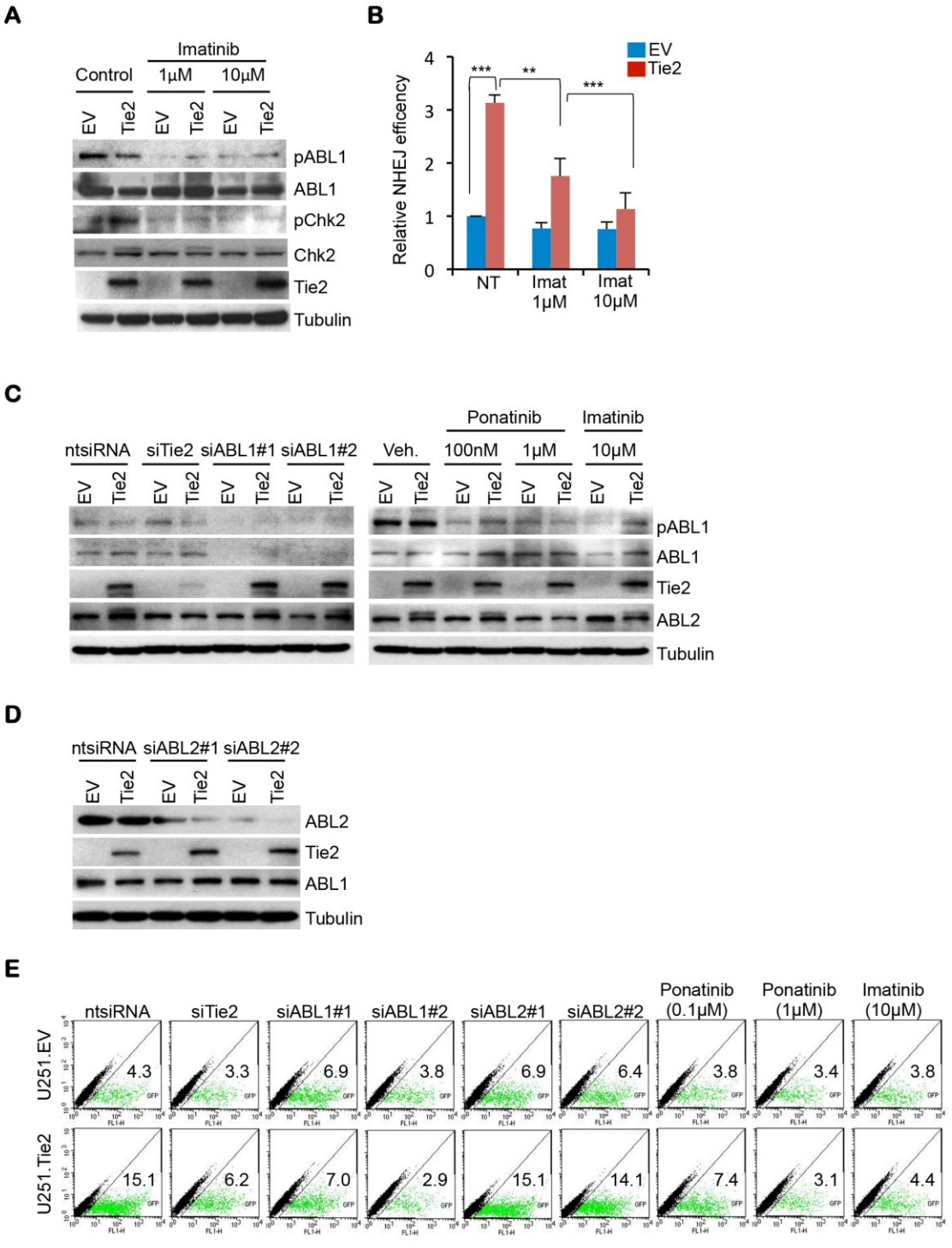

Figure S16. Additional analysis on TIE2/ABL1 axes in NHEJ repair

fig. S16. Additional analysis on TIE2/ABL1 axes in NHEJ repair. (**A** and **B**) Imatinib inhibits TIE2-mediated NHEJ DNA repair. (**A**) Whole cell lysates were immunoblotted to analyze the effect of Imatinib on total and phosphorylated forms of ChK2 and ABL1. (**B**) NHEJ reporter plasmid, *Hind*III-linearized pEGFP-Pem1-Ad2, was transfected into U251.EV and U251.Tie2 cells. 24 h later, cultures were treated with imatinib at the indicated concentrations for 24 h. NHEJ efficiency was analyzed by FACS-guided quantification of EGFP-positive cells normalized to Ds-Red-positive cells. Data represent mean ± s.d. $^{**}P \leq 0.01$, $^{***}P \leq 0.001$. (**C**) Immunoblot of whole cell lysates derived from U251.EV and U251.Tie2 cells after transfection with 10nM siRNAs against TIE2 or ABL1, or treatment with ponatinib or imatinib at the indicated doses. (**D**) Immunoblot of whole cell lysates derived from U251.EV and U251.Tie2 cells following transfection with 10nM siRNAs against ABL2. (**E**) Inhibition of ABL1, but not ABL2, resulted in abrogation of TIE2-mediated NHEJ DNA repair. U251.EV and U251.Tie2 cells were transfected with 10nM siRNAs against TIE2, ABL1, or ABL2, or treated with ponatinib or imatinib at the indicated concentrations. 24 h later, cells were transfected with the *Hind*III linearized pEGFP-Pem1-Ad2 plasmid. NHEJ efficiency was quantified as the percentage of EGFP-positive cells normalized to Ds-Red-positive cells.

Table S1. List of siRNA sequences used for this study.

Target protein	**Company**	**5´ to 3´ Sequence**
TIE2 (TIE2#1)	Life technology ID: s13984; No. 4390824	S : GCUUCUAUACAAACCCGUUtt As: AACGGGUUUGUAUAGAAGCtt
TIE2 (TIE2#2)	Santa Cruz Biotechnology No. sc-36677	• S: GCUACCUACUAAUGAAGAAtt As: UUCUUCAUUAGUAGGUAGCtt • S: CAGGAGAACUGGAAGUUCUtt As: AGAACUUCCAGUUCUCCUGtt • S: CUGGUAAUAUUGACUUGUAtt As: UACAAGUCAAUAUUACCAGtt
ABL1 (ABL1#1)	Life technology ID: s866; No. 4390824	S : CACUCUAAGCAUAACUAAAtt As: UUUAGUUAUGCUUAGAGUGtt
ABL1 (ABL1#2)	Life technology ID: s865; No. 4390824	S : CGACAAGUGGGAGAUGGAAtt As: UUCCAUCUCCCACUUGUCGta
ABL2 (ABL2#1)	Life technology ID: s229383; No. 4392420	S : CCUAUGGAAUGUCACCAUAtt As: UAUGGUGACAUUCCAUAGGta
ABL2 (ABL2#2)	Life technology ID: s229384; No. 4392420	S : CUAGAAAAAGGAUAUCGAAtt As: UUCGAUAUCCUUUUUCUAGta

Table S2. List of primer sequences.

Primer Name	5´ to 3´ Sequence
Tie2 d580-586 F	GATGACTTTTATGTTGAAGTGGAGGATCAGCAGAATATTAAAGTTCCA
Tie2 d580-586 R	TGGAACTTTAATATTCTGCTGATCCTCCACTTCAACATAAAAGTCATC
Tie2 RR580/81AA F	AGATGACTTTTATGTTGAAGTGGAGGCAGCGTCTGTGCAAAAAAGTGATCAGCAG
Tie2 RR580/81AA R	CTGCTGATCACTTTTTTGCACAGACGCTGCCTCCACTTCAACATAAAAGTCATCT
Tie2 K585A F	GAAGTGGAGAGAAGGTCTGTGCAAGCAAGTGATCAGCAGAATATTAAAG
Tie2 K585A R	CTTTAATATTCTGCTGATCACTTGCTTGCACAGACCTTCTCTCCACTTC
Tie2 d585-586 F	GGAGAGAAGGTCTGTGCAAGATCAGCAGAATATTAAAG
Tie2 d585-586 R	CTTTAATATTCTGCTGATCTTGCACAGACCTTCTCTCC
Tie2 SS582/86AA F	GAAGTGGAGAGAAGGGCTGTGCAAAAAGCTGATCAGCAGAATATTAAAG
Tie2 SS582/86AA R	CTTTAATATTCTGCTGATCAGCTTTTTGCACAGCCCTTCTCTCCACTTC
Tie2 S582A F	GTTGAAGTGGAGAGAAGGGCTGTGCAAAAAAGTGATC
Tie2 S582A R	GATCACTTTTTTGCACAGCCCTTCTCTCCACTTCAAC
Tie2 S586A F	GAAGTGGAGAGAAGGTCTGTGCAAAAAGCTGATCAGCAGAATATTAAAG
Tie2 S586A R	CTTTAATATTCTGCTGATCAGCTTTTTGCACAGACCTTCTCTCCACTTC
Tie2 (RT PCR) F	TTACGGGCCAGATTGTAAGC
Tie2 (RT PCR) R	CATCCCCAAAGTAAGGCTCA
GAPDH (RT PCR) F	ATGGGGAAGGTGAAGGTCGG
GAPDH (RT PCR) R	GACGGTGCCATGGAATTTGC
Ang1 (RT-PCR) F	AGAGAAGCAACTTCTTCAACAGACAA
Ang1 (RT-PCR) R	CAAAACCCATTTTATATTCCTTCCAG
Ang1 (qRT-PCR) F	CCTGATCTTACACGGTGCTG
Ang1 (qRT-PCR) R	ATCAAACCACCATCCTCCTG
β-actin (qRT-PCR) F	GCATCCACGAAACTACCTTCAAC

β-actin (qRT-PCR) R	ACTGTGTTGGCGTACAGGTCTTT
Tie2-myc (dKD) F	AGGGCAAATGTGCAAAGGAGAGGGTCCGAACA
Tie2-myc (dKD) R	TGTTCGGACCCTCTCCTTTGCACATTTGCCCT
Tie2-myc K855A F	TACGGATGGATGCTGCCATCGCAAGAATGAAAGAATATGCCTC
Tie2-myc K855A R	GAGGCATATTCTTTCATTCTTGCGATGGCAGCATCCATCCGTA

Table S3. List of antibodies used for this study.

Antibody	Company	Experimental use
TIE2 (C-20)	Santa Cruz Biotechnology Inc. (No. sc-324)	WB (1:2000) IP IF (1:500)
TIE2 (H176)	Santa Cruz Biotechnology Inc. (No. sc-9026)	WB (1:2000)
PE-conjugated Tie2 (mouse)	R&D Systems (No. FAB3131P)	FACS
PE-conjugated IgG (mouse)	BD Biosciences (No. 340761)	FACS
LaminB	Santa Cruz Biotechnology Inc. (No. sc-6216)	WB (1:4000)
ALPHA-Tubulin	Santa Cruz Biotechnology Inc. (No. sc-23948)	WB (1:5000)
DNA-PK	Santa Cruz Biotechnology Inc. (No. sc-9051)	WB (1:2000)
BRG1	Santa Cruz Biotechnology Inc. (No. sc-10768)	WB (1:2000)
Phospho-TIE2 (Tyr992)	Cell Signaling Technology (No. 4221)	WB (1:500)
MYC-tag	Cell Signaling Technology (No. 2276)	WB (1:2000) IP IF (1:500)
γH2AX (mouse)	Abcam (No. ab26350)	WB (1:2000) IF (1:1000)
γH2AX (rabbit)	Abcam (No. ab2893)	IP
Anti-Flag M2	Sigma Aldrich (No. F3165)	WB (1:2000) IP
Mouse TrueBlot ULTRA: Anti-Mouse Ig HRP	Rockland (No. 18-1877-33)	WB (1:2000)
Alexa Fluor 555 Goat Anti-	Life Technologies	IF (1:1000)

Rabbit IgG (H+L)	(No. A-21429)	
Alexa Fluor 555 Goat Anti-Mouse IgG (H+L)	Life Technologies (No. A-21422)	IF (1:1000)
Alexa Fluor 488 Goat Anti-Mouse IgG (H+L)	Life Technologies (No. A-11029)	IF (1:1000)
Alexa Fluor 488 Goat Anti-Rabbit IgG (H+L)	Life Technologies (No. A-11070)	IF (1:1000)
ABL1 (cAbl)	Cell Signaling Technology (No. 2862)	WB (1:2000)
ABL1 (cAbl)	Abcam (No. ab85947)	IF (1:50)
Phospho-ABL1 (Tyr245)	Cell Signaling Technology (No. 2861)	WB (1:1000)
ABL2	Abcam (No. ab134134)	WB (1:2000)
ATM	Abcam (No. ab81292)	WB (1:2000)
Phospho-ATM (Ser1981)	Abcam (No. ab78)	WB (1:2000)
HISTONE H3	Abcam (No. ab1791)	WB (1:2000)
HISTONE H4	Abcam (No. ab1791)	WB (1:2000)
Phosphotyrosine (PY20)	Abcam (No. ab10321)	WB (1:1000)
CHK2	Millipore (No. 05-649)	WB (1:2000)
Phospho-CHK2 (Thr68)	Cell Signaling Technology (No. 2661)	WB (1:1000)
ANG1	R&D Systems (No. AF923)	WB (1:2000) IF (1:250)
Acetyl-LYSINE (clon4G12)	Millipore (No. 05-515)	WB (1:1000)

Phospho-H3 (S28)	Abcam (No. ab5169)	WB (1:1000)
Ku70 [N3H10]	Abcam (No. ab3114)	WB (1:2000)
Ku80 [5C5]	Abcam (No. ab119935)	WB (1:2000)
HIS-tag	Sigma (No. H1029)	WB (1:2000)
Biotinylated anti-rabbit IgG	Vector Labs (No. BA-1000)	IF (1:500)
DyLight594-conjugated streptavidin	Vector Labs (No. SA-5594-1)	IF (1:500)
Biotinylated anti-streptavidin	Vector Labs (No. BA-0500)	IF (1:500)
Clean-Blot™ IP Detection Reagent (HRP)	Life Technologies (No. 21230)	WB (1:1000)

WB – Western blotting; IP – Immunoprecipitation; IF – Immunofluorescence; dilutions of antibodies are given in brackets.